

Event horizon image within black hole shadow

V.I. Dokuchaev,^{a,b,1} and N.O. Nazarova^b

^aInstitute for Nuclear Research of the Russian Academy of Sciences, Moscow, 117312 Russia

^bNational Research Nuclear University MEPhI (Moscow Engineering Physics Institute), Moscow, 115409 Russia

E-mail: dokuchaev@inr.ac.ru, nazarova.mephi@gmail.com

Abstract. The external border of the black hole shadow is washed out by radiation from matter plunging into black hole and approaching the event horizon. This effect will crucially influence the results of future observations by the Event Horizon Telescope. We show that gravitational lensing of the luminous matter plunging into black hole provides the event horizon visualization within black hole shadow. The lensed image of the event horizon is formed by the last highly red-shifted photons emitted by the plunging matter and viewed by a distant observer. The resulting event horizon image is a gravitationally lensed projection on the sky plane of the whole black hole event horizon sphere. Seemingly, black holes are the unique objects in the Universe which may be viewed by distant observers at once from both the front and back sides.

¹Corresponding author.

Contents

1	Introduction	1
2	Black hole shadow	2
3	Event horizon image	4
4	Conclusion	7

1 Introduction

The supermassive black hole SgrA* at the Galactic Center with a mass $M = (4.3 \pm 0.3)10^6 M_\odot$ [1–6] is the object of especially steadfast investigations. The one reason is that this black hole is the nearest “dormant” quasar dwelling precisely at the center of our native Galaxy. The other reason is that nowadays there are technologies permitting to view the enigmatic black hole directly for the first time. The Event Horizon Telescope, a global network of mm and sub-mm telescopes [7–15], intends to reveal the shadow of supermassive black hole at the Galactic Center [16–26]. It would be the first direct experimental verification (or falsification) of the very existence of black holes in the Universe.

The black hole shadow is formed by gravitational lensing of luminous background, consisting of bright stars or hot gas, which are located either far enough from the black hole or at the stationary orbits around it. In other words, the apparent image of the black hole is a capture cross section of background photons viewed by distant observers on the celestial sphere.

A next stage in investigation of the black hole shadow at the Galactic Center would be the detailed elaboration of its shape for verification of the General Relativity in the strong field limit [27–36]. One of the promising interferometric projects for this future study is the proposed Russian Millimetron space interferometer project with an angular resolution of about one nanoarcsecond [37].

It is generally believed that the black hole event horizon is invisible and cannot be imaged within the black hole shadow. We show below that gravitational lensing of the luminous matter plunging into black hole provides in principle a possibility for visualization of the event horizon within the black hole shadow. The resulting image is a gravitationally lensed projection on the sky plane of the whole black hole event horizon sphere. Seemingly, black holes are the unique objects in the Universe which may be viewed by distant observers at once from both the front and back sides.

It is convenient to use units with the gravitational constant $G = 1$ and the velocity of light $c = 1$. With these units we define the dimensionless values of space distances, $r \Rightarrow r/M$, and time intervals, $t \Rightarrow t/M$ and the dimensionless spin parameter of the Kerr space-time for rotating black hole, $0 \leq a = J/M^2 \leq 1$, where M and J are, respectively, the black hole mass and angular momentum. The event horizon radius in the Kerr space-time is $r_h = 1 + \sqrt{1 - a^2}$. At $a = 0$ the Kerr space-time coincides with the Schwarzschild one. For numerical calculations of gravitational lensing in the Kerr space-time background we use

the integral equations of motion for photons [17, 38–41] in Boyer–Lindquist coordinates [42]:

$$\oint \frac{dr}{\sqrt{V_r}} = \oint \frac{d\theta}{\sqrt{V_\theta}}, \quad (1.1)$$

$$\phi = \oint \frac{a[E(r^2 + a^2) - La]}{(r^2 - 2r + a^2)\sqrt{V_r}} dr + \oint \frac{L - aE \sin^2 \theta}{\sin^2 \theta \sqrt{V_\theta}} d\theta,$$

where

$$V_r = [E(r^2 + a^2) - aL]^2 - \Delta[\mu^2 r^2 + (L - aE)^2 + Q], \quad (1.2)$$

$$V_\theta = Q - \cos^2 \theta [a^2(\mu^2 - E^2) + L^2 \sin^{-2} \theta]. \quad (1.3)$$

are, respectively, the latitudinal and radial effective potentials. There are four constants of motion for a test particle in the Kerr metric: mass μ , total energy E , azimuthal angular momentum L and Carter constant Q , defining the non equatorial motion. The integrals in (1.1) are understood to be path integrals along the test particle trajectory connecting a source to an observer.

Trajectories of massive particles ($\mu \neq 0$) in the Kerr space-time are determined by three parameters (constants of motion): $\gamma = E/\mu$, $\lambda = L/E$ and $q = \sqrt{Q}/E$. The corresponding trajectories of photons (null geodesics) are determined by two parameters, λ and q , which coincide with the horizontal and vertical impact parameters of photons on the celestial plane for a distant observer in the black hole equatorial plane. The Boyer–Lindquist coordinates, which we use in numerical calculations of photon trajectories, coincide asymptotically at $r \rightarrow \infty$ with the flat Euclidean spherical coordinates.

See [43–47] for corresponding examples of analytical computations for null geodesics in the Kerr space-time. An example of numerical gravitational lensing animation of the compact star orbiting the rotating black hole see at [48, 49].

2 Black hole shadow

The apparent shape of the black hole shadow, as seen by a distant observer in the equatorial plane, is determined parametrically, $(\lambda, q) = (\lambda(r), q(r))$, from simultaneous solution of equations $V_r(r) = 0$ and $[rV_r(r)]' = 0$ [16, 17]:

$$\lambda = \frac{-r^3 + 3r^2 - a^2(r + 1)}{a(r - 1)}, \quad (2.1)$$

$$q^2 = \frac{r^3[4a^2 - r(r - 3)^2]}{a^2(r - 1)^2}. \quad (2.2)$$

The shadow of Schwarzschild black hole ($a = 0$) is shown in figure 1 (left panel). The largest (purple) disk is the black hole shadow with a radius $r_{\text{sh}} = 3\sqrt{3} \simeq 5.196$. The blue disk at the shadow center is a fictitious event horizon image in the imaginary Euclidean space. The corresponding shadow of extreme Kerr black hole ($a = 1$) is shown in figure 1 (right panel). It is also shown the photon trajectory (multicolored 3D curve) near the shadow boundary (with $\lambda = 0$ and $q = \sqrt{3 - \sqrt{2}(1 + \sqrt{2})^{3/2}} \simeq 4.72$), starting from a distant background and reaching a distant observer in the equatorial plane. This photon has a radial turning point at $r_{\text{min}} = 1 + \sqrt{2}$. A vertical arrow is the black hole rotation axes. Inside the shadow it is shown

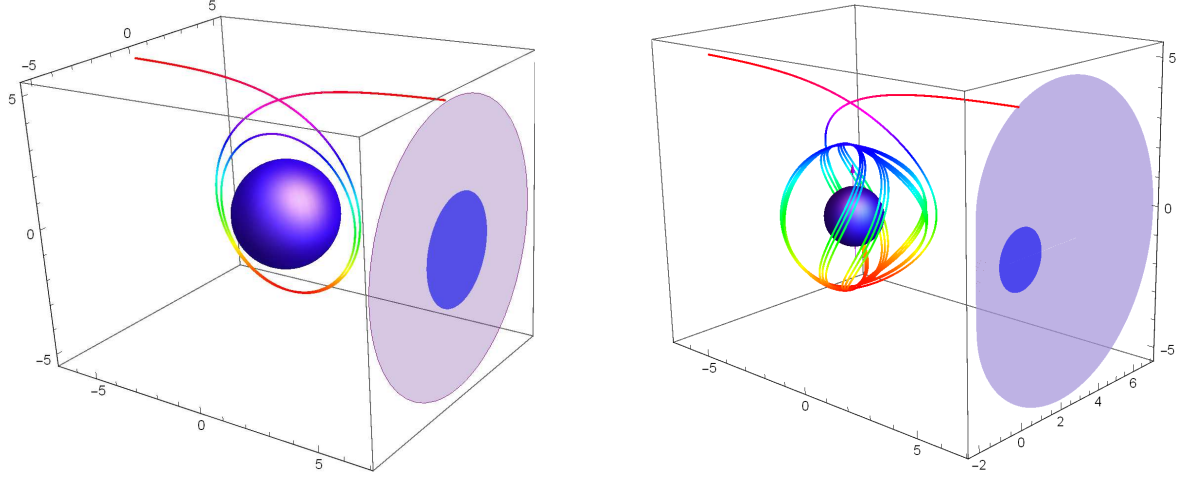


Figure 1. Left panel: The shadow (purple disk) of Schwarzschild black hole ($a = 0$) with a radius $r_{\text{sh}} = 3\sqrt{3} \approx 5.196$. Inside the shadow it is shown the fictitious image (blue disk) of the event horizon with radius $r_h = 2$ in the imaginary Euclidean space. It shown the photon trajectory (multicolored 3D curve) near the shadow boundary (with impact parameters $\lambda = 0$ and $q = 3\sqrt{3}$), starting from a distant background, winding near a radial turning point at $r_{\text{min}} = 3$ around the black hole event horizon (blue sphere) and reaching finally a distant observer in the equatorial plane. Left panel: The shadow (purple region) of the extremely fast rotating Kerr black hole ($a = 1$). As a representative example it is shown the photon trajectory (multicolored 3D curve) near the shadow boundary (with $\lambda = 0$ and $q = \sqrt{3 - \sqrt{2}(1 + \sqrt{2})^{3/2}} \approx 4.72$), starting from a distant background, winding around the black hole event horizon (blue sphere) and reaching a distant observer in the equatorial plane. This photon has a radial turning point at $r_{\text{min}} = 1 + \sqrt{2}$. A vertical magenta arrow is the black hole rotation axis. Inside the shadow it is shown the fictitious image (blue disk) of the event horizon with radius $r_h = 1$ in the imaginary Euclidean space.

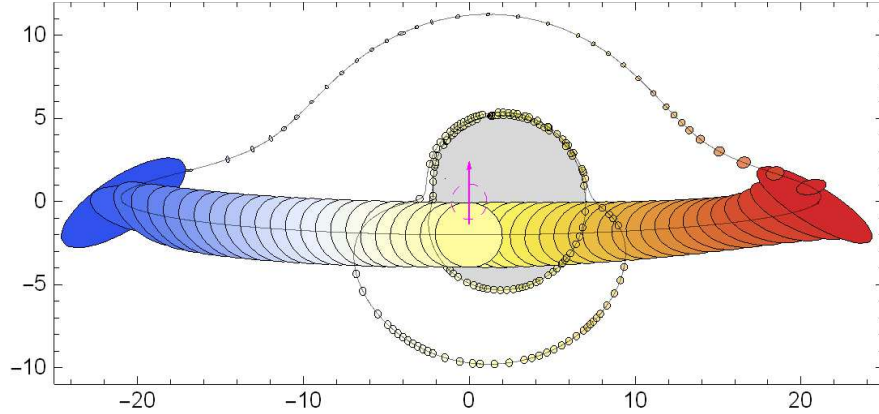


Figure 2. Gravitational lensing of a compact prob (star) orbiting the rotating black in the equatorial plane at radius $r = 20$ and viewed by a distant observer. A distant observer is situated above the equatorial plane at $\cos \theta = 0.1$. Direct star images and also the first and second light echoes around the black hole shadow (filled gray region) are shown in discrete time intervals. For details see [48, 49].

the fictitious image (blue disk) of the event horizon with radius $r_h = 1$ in the imaginary Euclidean space. See in figure 2 the numerical simulation of the image of a compact probe

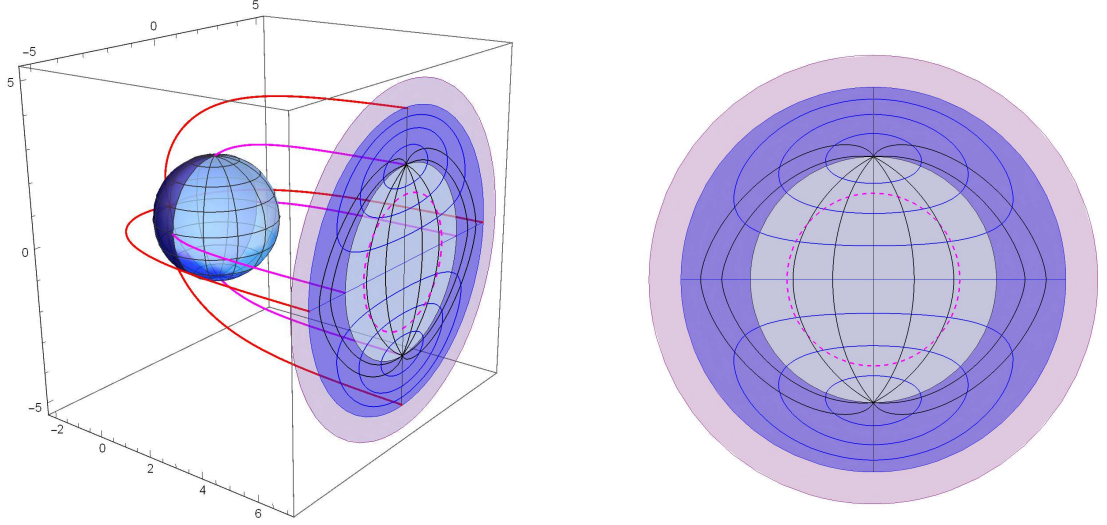


Figure 3. Left panel: The event horizon image (blue disk) inside the black hole shadow (purple disk) in the Schwarzschild case ($a = 0$). The dashed magenta circle here and on the subsequent Figs. is a fictitious outer border of the event horizon image in the imaginary Euclidean space. The trajectories of some photons forming the event horizon image are shown: 4 (red colored) trajectories with $\sqrt{\lambda^2 + q^2} = r_{\text{eh}}$ are starting from the farthest point of the event horizon globe, and, respectively, 4 (magenta colored) trajectories with $\sqrt{\lambda^2 + q^2} = r_{\text{EW}}$ are starting from the East-West meridian. Images of some parallels (blue curves) and meridians (black curves) are also shown on the event horizon globe (blue sphere) and on its projected image (blue region) viewed by distant observer. The light-blue part of the event horizon image is a projection of the nearest event horizon hemisphere. Respectively, the dark-blue part of the event horizon image is a projection of the farthest event horizon hemisphere. A distant observer views the event horizon at once from both the front and back sides. Right panel: The detailed view of the event horizon image inside black hole shadow.

(star) orbiting around rotating black hole.

3 Event horizon image

In the vicinity of a black hole, like the SgrA*, besides the near stationary foreground matter, there may be the non-stationary luminous objects (compact gas clouds and stars), plunging into black hole. These luminous objects will inevitably washing out the outer border of the observable black hole shadow.

It is useful to imagine the gedankenexperiment of throwing the luminous probes in all directions and from every quarter into the black hole. A distant observer will see the progressively weakened image of each plunging probe, approaching the event horizon with the redshift of emitting photons growing to infinity for the “last” photon. Position of the last lensed photon on the celestial sky, determined by the tracking of the separate plunging probe, will map the single point on the event horizon. The set of these points would be the one-to-one projection of the whole event horizon sphere into its lensed image. The last detected highly red-shifted photons will mark the specific final points on the event horizon image.

In result, the limiting process of registration the progressively fading images of plunging luminous probes (like the compact stars and hot clouds) provides the event horizon

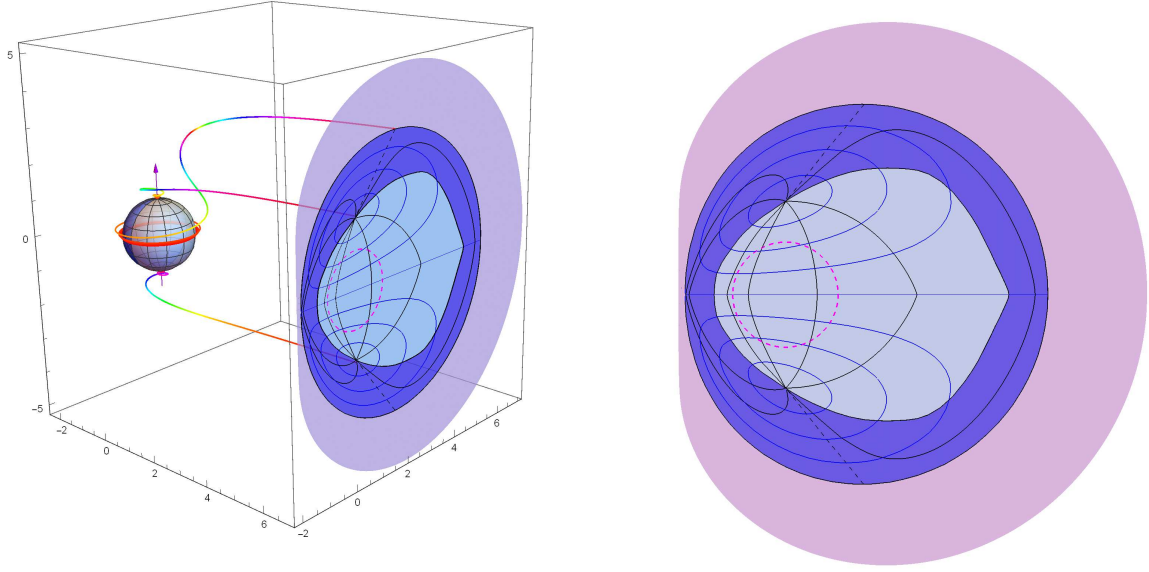


Figure 4. Left panel: The event horizon image of extreme Kerr black hole ($a = 1$) and trajectories (multicolored 3D curves) of some photons forming this image and outgoing to a distant observer from the North and South poles (with $\lambda = 0$, $q = 1.77$) and from the equator (with $\lambda = -1.493$, $q = 3.629$) of the event horizon globe with a radius $r_h = 1$. The largest purple region is the black hole shadow. Images of some parallels (blue curves) and meridians (black curves) are also shown on the event horizon globe (blue sphere) and on its projected image (blue region) viewed by distant observer. The light-blue part of the event horizon image is a projection of the nearest event horizon hemisphere. Respectively, the dark-blue part of the event horizon image is a projection of the farthest event horizon hemisphere. A distant observer views the event horizon at once from both the front and back sides. Left panel: The detailed view of the event horizon image of extreme Kerr black hole.

mapping into its viewed image. It is crucial that this image is a complete one-to-one projection of the whole event horizon sphere. This unique property of the event horizon image means that any distant observer may view at once the black hole on all sides. The lensed event horizon image is placed entirely within the black hole shadow.

In figure 3 the trajectories of some photons forming the event horizon image of the Schwarzschild black hole are shown, which are starting just above the event horizon globe: 4 (red colored) trajectories with $\sqrt{\lambda^2 + q^2} = r_{\text{eh}}$ are starting from the farthest point, and 4 (magenta colored) trajectories with $\sqrt{\lambda^2 + q^2} = r_{\text{EW}}$ are starting from the East-West meridian. Images of some parallels and meridians of the event horizon globe are also shown. A distant observer views at once both the front and back sides of the event horizon.

The outer boundary of event horizon image, viewed by a distant observer in the equatorial plane, is defined by solving the integral equation

$$\int_2^\infty \frac{dr}{\sqrt{V_r}} = 2 \int_{\theta_{\min}}^{\pi/2} \frac{d\theta}{\sqrt{V_\theta}}. \quad (3.1)$$

where θ_{\min} is a turning point in the latitudinal θ -direction on the photon trajectory for direct image, defined from equation $V_\theta = 0$. Photons, producing the direct image in the

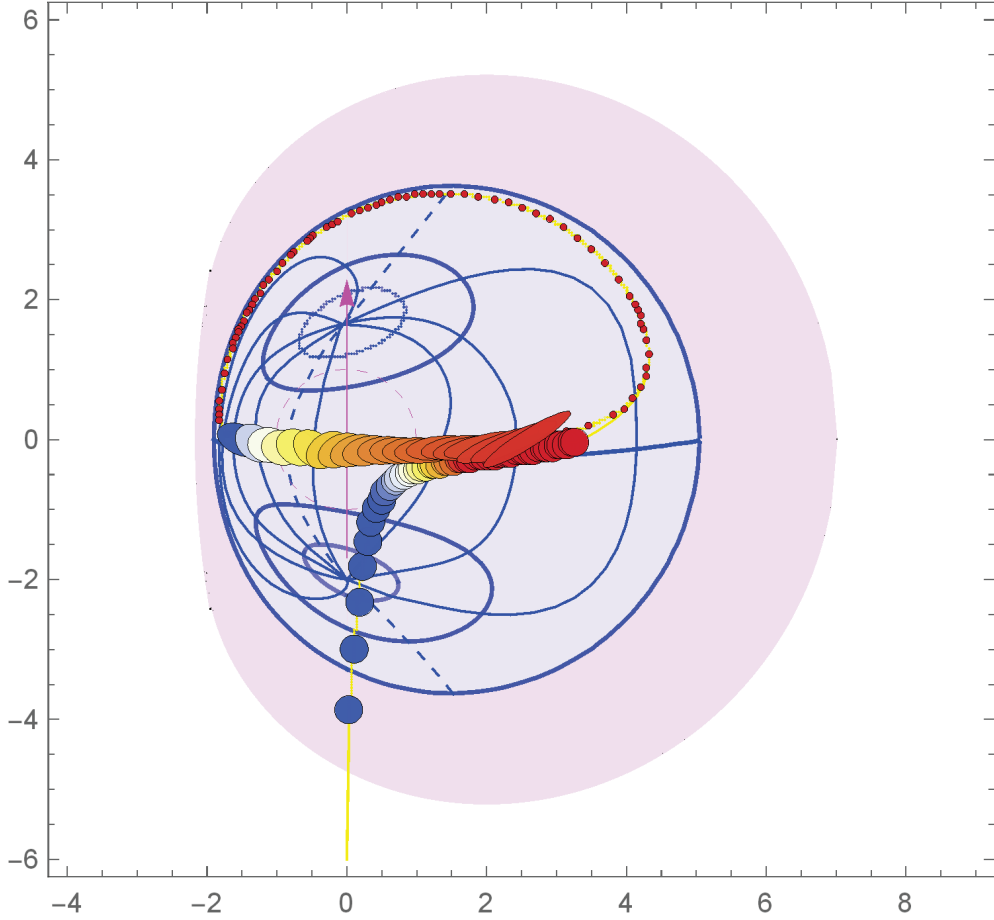


Figure 5. Numerical simulation of the lensed images of the spherical compact star with orbital parameters $\gamma = 1$, $\lambda = q = 0$ plunging into rotating black hole with $a = 0.998$ at the equatorial plane and shown in discrete time intervals. A distant observer is placed above the equatorial plane at $\cos \theta = 0.1$. The lensed images are winding around black hole at the equatorial parallel $\theta = \pi/2$ of the event horizon globe when plunging star is approaching the event horizon. It is shown the first circle of this winding within the black hole shadow (purple disk). See numerical animation of this gravitational lensing at [51].

Cunningham–Bardeen classification scheme for multiple lensed images [50], do not intersect the black hole equatorial plane on the way from emitting probe to a distant observer.

In the simplest spherically symmetric Schwarzschild case ($a=0$) the event horizon sphere has radius $r_h = 2$, a turning point $\theta_{\min} = \arccos(q/\sqrt{q^2 + \lambda^2})$. A corresponding value of the right-hand-side integral in (3.1) is $\pi/\sqrt{q^2 + \lambda^2}$. In result, from numerical solution of integral equation (3.1) we find the radius of the event horizon image $r_{\text{eh}} = \sqrt{q^2 + \lambda^2} = 4.457$. The near hemisphere of the event horizon with a radius $r_h = 2$ is projected by the lensing photons into the central (light blue) disk of the image with a radius $r_{\text{EW}} \simeq 2.848$. Respectively the far hemisphere is projected into the hollow (dark blue) disk with an outer radius $r_{\text{eh}} \simeq 4.457$, which is a radius of the event horizon image. The event horizon image is placed within the black hole shadow.

In the general axially symmetric Kerr case, when $a \neq 0$, a turning point in θ -direction

is

$$\theta_{\min} = \arccos \left[\sqrt{\frac{\sqrt{4a^2q^2 + (q^2 + \lambda^2 - a^2)^2} - (q^2 + \lambda^2 - a^2)}{2a^2}} \right], \quad (3.2)$$

and the event horizon image has a more complicated form. The corresponding numerical solution of integral equation (3.1) for the outer boundary of the event horizon image of the extreme Kerr black hole ($a = 1$) is presented graphically in figure 4. The near hemisphere of the event horizon is projected by the lensing photons into the central (light blue) region. Respectively the far hemisphere is projected into the hollow (dark blue) region. Images of some parallels and meridians of the event horizon globe are also shown.

The black hole horizon and its image are both synchronously rotating as a solid body with an angular velocity

$$\Omega_h = \frac{a}{2(1 + \sqrt{1 - a^2})}. \quad (3.3)$$

Additionally the plunging test probes are infinitely winding in ϕ direction by approaching the event horizon if $a \neq 0$. This very specific feature of the rotating black hole complicates the procedure for fixation of meridians on the event horizon image. By definition, the lensed image of meridians on the rotating event horizon globe are marked by photons, emitting at the same radii along the chosen meridian, $r = r_h + \epsilon$ and $\epsilon = \text{const} \ll 1$, i. e., very close but still a little bit above the event horizon at $r = r_h$. Once being marked, these lensed image of meridian will be rotating synchronously with both the event horizon globe and event horizon image.

See in figure 5 the lensed images of a compact star plunging at the equatorial plane into a fast rotating black hole and shown in discrete time intervals (from numerical animation [51]). The lensed images of this plunging star mark at final stages the equatorial parallel of the event horizon globe on the event horizon image inside black hole shadow.

4 Conclusion

We show that gravitational lensing of the luminous matter plunging into black hole provides the event horizon visualization within black hole shadow. A real visualization of the black hole event horizon by means of astrophysical observations is an extremely complicated problem. New technological solutions are requested for mining the highly red-shifted photons deeply buried inside the black hole shadow.

We finally conclude that a genuine image of the black hole is not its shadow, produced by the luminous stationary background, but a more compact event horizon image, highlighted by the luminous non-stationary matter plunging into black hole. The resulting event horizon image is a gravitationally lensed projection on the sky plane of the whole black hole event horizon sphere. Seemingly, black holes are the unique objects in the Universe which may be viewed by distant observers at once from both the front and back sides.

Acknowledgments

We are grateful to E.O. Babichev, V.A. Berezin, Yu.N. Eroshenko and A.L. Smirnov for stimulating discussions.

This work was supported in part by grant No. 18-52-15001 from Russian Foundation for Basic Research (RFBR) and Centre National de la Recherche Scientifique (CNRS).

References

- [1] S. Gillessen, F. Eisenhauer, S. Trippe, T. Alexander, R. Genzel, F. Martins and T. Ott, *Monitoring stellar orbits around the Massive Black Hole in the Galactic Center*, *Astrophys. J.* (2009) **692** 1075 [arXiv:0810.4674].
- [2] L. Meyer, A.M. Ghez, R. Schoedel, S. Yelda, A. Boehle, J.R. Lu, T. Do, M.R. Morris, E.E. Becklin and K. Matthews, *The shortest known period star orbiting our Galaxy’s supermassive black hole*, *Science* (2012) **338** 84 [arXiv:1210.1294].
- [3] M.D. Johnson et al. *Resolved magnetic-field structure and variability near the event horizon of Sagittarius A**, *Science* (2015) **350** 1242 [arXiv:1512.01220].
- [4] S. Chatzopoulos, T. Fritz, O. Gerhard, S. Gillessen, C. Wegg, R. Genzel and O. Pfuhl, *The old nuclear star cluster in the Milky Way: dynamics, mass, statistical parallax, and black hole mass*, *Mon. Not. R. Astron. Soc.* (2015) **447** 948 [arXiv:1403.5266].
- [5] T. Johannsen, *Sgr A* and General Relativity* *Class. Quantum Grav.* (2016) **33** 113001 [arXiv:1512.03818].
- [6] A. Eckart, A. Huettemann, C. Kiefer, S. Britzen, M. Zajacek, C. Laemmerzahl, M. Stockler, M. Valencia-S., V. Karas and M. Garcia-Marin, *The Milky Way’s supermassive black hole: how good a case is it? A challenge for astrophysics and philosophy of Science*, *Foundations of Physics* (2017) **47** 553 [arXiv:1703.09118].
- [7] V.L. Fish, K. Akiyama, K.L. Bouman, A.A. Chael, M.D. Johnson, S.S. Doeleman, L. Blackburn, J.F.C. Wardle, W.T. Freeman, the Event Horizon Telescope Collaboration *Observing—and Imaging—Active Galactic Nuclei with the Event Horizon Telescope*, *Galaxies* (2016) **4** 54 [arXiv:1607.03034].
- [8] T. Lacroix and J. Silk, *Constraining the distribution of dark matter at the Galactic centre using the high-resolution Event Horizon Telescope*, *Astron. Astrophys.* (2013) **554** A36 [arXiv:1211.4861].
- [9] T. Johannsen, A.E. Broderick, P.M. Plewa, S. Chatzopoulos, S.S. Doeleman, F. Eisenhauer, V.L. Fish, R. Genzel, O. Gerhard and M.D. Johnson, *Testing General Relativity with the shadow size of Sgr A**, *Phys. Rev. Lett.* (2016) **116** 031101 [arXiv:1512.02640].
- [10] T. Johannsen, C. Wang, A.E. Broderick, S.S. Doeleman, V.L. Fish, A. Loeb and D. Psaltis, *Testing General Relativity with accretion-flow imaging of Sgr A**, *Phys. Rev. Lett.* (2016) **117** 091101 [arXiv:1608.03593].
- [11] A.E. Broderick, V.L. Fish, M.D. Johnson, K. Rosenfeld, C. Wang, S.S. Doeleman, K. Akiyama, T. Johannsen and A.L. Roy *Modeling seven years of Event Horizon Telescope observations with radiatively inefficient accretion flow models*, *Astrophys. J.* (2016) **820** 137 [arXiv:1602.07701].
- [12] A.A. Chael, M.D. Johnson, R. Narayan, S.S. Doeleman, J.F.C. Wardle and K.L. Bouman, *High resolution linear polarimetric imaging for the Event Horizon Telescope*, *Astrophys. J.* (2016) **829** 11 [arXiv:1605.06156].
- [13] J. Kim, D.P. Marrone, C. Chan, L. Medeiros, F. Özel and D. Psaltis, *Bayesian techniques for comparing time-dependent GRMHD simulations to variable Event Horizon Telescope observations*, *Astrophys. J.* (2016) **832** 156 [arXiv:1602.00692].
- [14] F. Roelofs, M.D. Johnson, H. Shiokawa, S.S. Doeleman and H. Falcke, *Quantifying intrinsic variability of Sagittarius A* using closure phase measurements of the Event Horizon Telescope* *Astrophys. J.* (2017) **847** 55 [arXiv:1708.01056].
- [15] S. Doeleman, *Seeing the unseeable*, *Nature Astron.* **1** 646 [arXiv:1710.03104].
- [16] J.M. Bardeen, in *Black Holes*, Eds. C. DeWitt, B.S. DeWitt, New York: Gordon and Breach (1973), pg. 219.
- [17] S. Chandrasekhar, *The Mathematical Theory of Black Holes*, Oxford: Clarendon Press (1983).

- [18] H. Falcke, F. Melia and E. Agol, *Viewing the Shadow of the Black Hole at the Galactic Center*, *Astrophys. J.* **528** (2000) L13 [arXiv:astro-ph/9912263].
- [19] R. Takahashi, *Shapes and Positions of Black Hole Shadows in Accretion Disks and Spin Parameters of Black Holes*, *Astrophys. J.* **611** (2004) 996 [arXiv:astro-ph/0405099].
- [20] H. Falcke and S. Markoff, *Towards the event horizon – the supermassive black hole in the Galactic Center*, *Class. Quantum Grav.* **30** (2013) 244003 [arXiv:1311.1841].
- [21] Z. Li and C. Bambi, *Measuring the Kerr spin parameter of regular black holes from their shadow*, *JCAP* **01** (2014) 041 [arXiv:1309.1606].
- [22] P.V.P. Cunha, C.A.R. Herdeiro, E. Radu and H.F. Runarsson, *Shadows of Kerr black holes with scalar hair*, *Phys. Rev. Lett.* **115** (2015) 211102 [arXiv:1509.00021].
- [23] A.A. Abdujabbarov, L. Rezzolla and B.J. Ahmedov, *A coordinate-independent characterization of a black hole shadow*, *Mon. Not. R. Astron. Soc.* **454** (2015) 2423 [arXiv:1503.09054].
- [24] Z. Younsi, A. Zhidenko, L. Rezzolla, R. Konoplya and Y. Mizuno, *A new method for shadow calculations: application to parameterised axisymmetric black holes*, *Phys. Rev. D* **94** (2016) 084025 [arXiv:1607.05767].
- [25] N.S. Kardashev, I.D. Novikov and A.A. Shatskiy, *Astrophysics of wormholes*, *Int. J. Mod. Phys. D* **16** (2007) 909 [arXiv:astro-ph/0610441].
- [26] O. James, E. von Tunzelmann, P. Franklin and K.S. Thorne, *Gravitational Lensing by Spinning Black Holes in Astrophysics, and in the Movie Interstellar*, *Class. Quantum Grav.* **32** (2015) 065001 [arXiv:1502.03808].
- [27] A. Shatskiy, I.D. Novikov and N.S. Kardashev, *New analytic models of traversable wormholes*, *Phys. Usp.* **51** (2008) 457 [arXiv:0810.0468].
- [28] E.O. Babichev, V.I. Dokuchaev and Yu.N. Eroshenko, *Black holes in the presence of dark energy*, *Phys. Usp.* **56** (2013) 1155 [arXiv:1406.0841].
- [29] V.I. Dokuchaev, *Spin and mass of the nearest supermassive black hole*, *Gen. Relativ. Grav.* **46** (2014) 1832 [arXiv:1306.2033].
- [30] V.I. Dokuchaev and Yu.N. Eroshenko, *Weighing of the Dark Matter at the Center of the Galaxy*, *JETP Lett.* **101** 777 [arXiv:1508.05725].
- [31] V.I. Dokuchaev and Yu.N. Eroshenko, *Physical laboratory at the center of the Galaxy*, *Phys. Usp.* **58** (2015) 772 [arXiv:1512.02943].
- [32] A. Herrera-Aguilar and U. Nucamendi, *Kerr black hole parameters in terms of red/blue shifts of photons emitted by geodesic particles*, *Phys. Rev. D* **92** (2015) 045024 [arXiv:1506.05182].
- [33] R. Becerril, S. Valdez-Alvarado and U. Nucamendi, *Obtaining mass parameters of compact objects from red-blue shifts emitted by geodesic particles around them*, *Phys. Rev. D* **94** (2016) 124024 [arXiv:1610.01718].
- [34] C.M. Will, M. Maitra, *Relativistic orbits around spinning supermassive black holes. Secular evolution to 4.5 post-Newtonian order*, *Phys. Rev. D* **95** (2017) 064003 [arXiv:1611.06931].
- [35] F. Ferrer, A. Medeiros da Rosa and C.M. Will *Dark matter spikes in the vicinity of Kerr black holes*, *Phys. Rev. D* **96** (2017) 083014 [arXiv:1707.06302].
- [36] C. Goddi, H. Falcke, M. Kramer et al., *BlackHoleCam: fundamental physics of the Galactic center* *Int. J. Mod. Phys. D* **26** (2017) 1730001 [arXiv:1606.08879].
- [37] N.S. Kardashev, I.D. Novikov, V.N. Lukash et al. *Review of scientific topics for Millimetron space observatory*, *Phys. Usp.* (2014) **57** 1199 [arXiv:1502.06071].
- [38] B. Carter, *Global structure of the Kerr family of gravitational fields*, *Phys. Rev.* **174** (1968) 1559.

- [39] F. de Felice, *Equatorial geodesic motion in the gravitational field of a rotating source*, *Nuovo Cim.* **57B** (1968) 351
- [40] J.M. Bardeen, W.H. Press and S.A. Teukolsky, *Rotating black holes: locally nonrotating frames, energy extraction, and scalar synchrotron radiation*, *Astrophys. J.* **178** (1972) 347.
- [41] C.W. Misner, K.S. Thorne and J.A. Wheeler, *Gravitation*, San Francisco, CA: Freeman (1973), pg. 901.
- [42] R.H. Boyer and R.W. Lindquist, *Maximal analytic extension of the Kerr Metric*, *J. Math. Phys.* **8** (1967) 265.
- [43] S.E. Gralla, A.P. Porfyriadis and N. Warburton, *Particle on the innermost stable circular orbit of a rapidly spinning black hole*, *Phys. Rev. D* **92** (2015) 064029 [arXiv:1506.08496].
- [44] S.E. Gralla, A. Lupsasca and A. Strominger, *Near-horizon Kerr magnetosphere*, *Phys. Rev. D* **93** (2016) 104041 [arXiv:1602.01833].
- [45] S.E. Gralla, A. Zimmerman and P. Zimmerman, *Transient Instability of Rapidly Rotating Black Holes*, *Phys. Rev. D* **94** (2016) 084017 [arXiv:1608.04739].
- [46] A.P. Porfyriadis, Y. Shi and A. Strominger, *Photon emission near extreme Kerr black holes*, *Phys. Rev. D* **95** (2017) 064009 [arXiv:1607.06028].
- [47] S.E. Gralla, A. Lupsasca and A. Strominger, *Observational signature of high spin at the Event Horizon Telescope*, *Mon. Not. R. Astron. Soc.* **475** (2018) 3829 [arXiv:1710.11112].
- [48] V.I. Dokuchaev and N.O. Nazarova, *Gravitational lensing of a star by rotating black hole*, *JETP Letters* **106** (2017) 637 [arXiv:1802.00817].
- [49] <https://youtu.be/P6DneV0vk7U>
- [50] C.T. Cunnungham and J.M. Bardeen, *The optical appearance of a star orbiting an extreme Kerr black hole*, *Astrophys. J.* **183** (1973) 237.
- [51] <https://youtu.be/P6DneV0vk7U>